To Reviewer #1 $\sim$ #9:

We greatly appreciate the reviewers for their constructive comments and suggestions. We have carried out exercises that the reviewers suggested and revised the manuscript accordingly. In addition to point-by-point responses, we would like to share the extended work we have done with all the reviewers.

This is the supplementary material for the paper entitled "Deep convolutional neural networks for uncertainty propagation in random fields". In particular, we would like to demonstrate the generalization of the proposed model by directly applying the network architecture to new problems including the Poisson's equation (Section 1.1) and Darcy's law (Section 1.2). Secondly, we have extended the current case study to the nonlinear range. Section 1.3 presents the modeling results of structures with nonlinear geometry. Thirdly, we have studied the model performance with different uncertainties. Section 1.4 presents the modeling results using Gaussian and non-Gaussian uncertainty models.

Poisson's Equation

To illustrate the effectiveness of the proposed surrogate to solve elliptic equations in general, we directly applied the network introduced in the first case to the following Poisson's equation:

$$-\left(u_{xx}+u_{yy}\right)=f(x,y) \quad \forall (x,y)\in\Omega\equiv(0,1)^2$$

The source term $f(x,y)$ is assumed to be a lognormal random field:

$$f(x,y)=\exp(GP(x,y)) \quad \text{where} \quad GP(x,y)\sim\mathcal{N}(m,k(\cdot,\cdot))$$

where $m=0$ and covariance function k is specified as:

$$k\left(\cdot,\cdot\right)=\exp\left(-\frac{(x-x')^2}{2\ell^2}\right)$$

where $\ell=1/2$. We are interested in developing the relationship between $f(x,y)$ and $u(x,y)$. We collected 1024 samples using finite difference method to train our surrogate, which takes the exact network architecture introduced in the first case study:

Layers	$N_{f(in)}$	$N_{f(out)}$	**Kernel**	**Stride**	**Padding**	**Dimension**
1	1	48	7	2	2	$31\times31\times48$
$2-6^{\dagger}$	48	16×5	3	1	1	$31\times31\times128$
7	128	64	3	2	1	$17\times17\times64$
$8-12^{\dagger}$	64	16×5	3	1	1	$17\times17\times144$
$13-14^{\ddagger}$	144	72	3	1	1	$32\times32\times72$
$15-18^{\dagger}$	72	18×4	3	1	1	$32\times32\times144$
$19-20^{\ddagger}$	144	144	3	1	1	$64\times64\times144$
21	144	1	3	1	1	$64\times64\times1$

Next, another 200 samples have been generated and used for testing. To show the prediction performance, 4 test samples are randomly selected and prediction results are summarized in the following figure. The prediction results suggest the proposed model can be effectively generalized to general elliptic systems, and confirm its efficiency regarding pixel-wise prediction tasks.

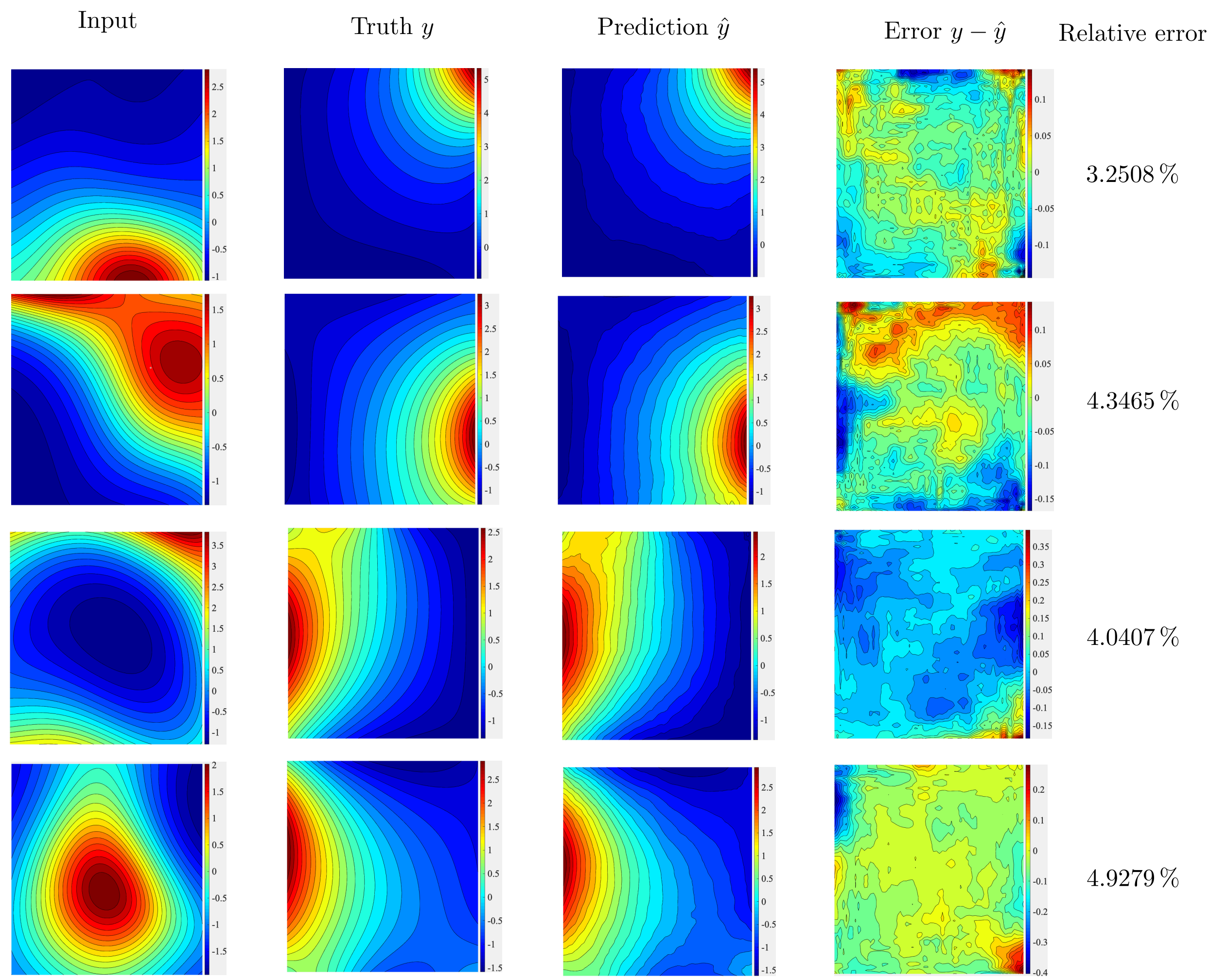

where the relative error is defined as:

$$\mathcal{E}\left(\mathbf{u}_{\mathrm{FR}}, \mathbf{u}_{\mathrm{FEM}}\right)=\frac{\left|\sum_{i=1}^{n_x} \sum_{j=1}^{n_y}\left|\mathbf{u}_{\mathrm{FEM}}\right|-\sum_{i=1}^{n_x} \sum_{j=1}^{n_y}\left|\mathbf{u}_{\mathrm{FR}}\right|\right|}{\sum_{i=1}^{n_x} \sum_{j=1}^{n_y}\left|\mathbf{u}_{\mathrm{FEM}}\right|}$$

Darcy's Law

In this example, we consider surrogate modeling of Darcy's law, which has been widely used to model for flow through a porous medium of some kind. Specifically, the governing equation for single phase fluid flow in a porous medium is given as:

$$\boldsymbol{q}=-\frac{K}{\mu}(\boldsymbol{\nabla} p-\rho g)$$

Here, K is the permeability, μ is the viscosity, ρ is the density of water, g is the gravitational constant, p is the pressure, and q models sources and sinks. For uncertainty analysis, we consider the random permeability field K on a unit square spatial domain. For the purposes of illustration and comparison, the same lognormal random field mentioned in the previous example is used.

In light of surrogate modeling, we are interested in approximating the relationship between $K(x, y)$ and $p(x, y)$. We trained our network using 1024 samples. For model validation, we tested our model using another 200 samples. Part of the prediction results are presented below. Again, computed results demonstrate the effectiveness of the proposed machine learning model. Note we have not done any architecture design or hyperparameter searching for this problem. Instead, we kept the network architecture implemented in the previous example. This indicates the developed network structure is highly optimized.

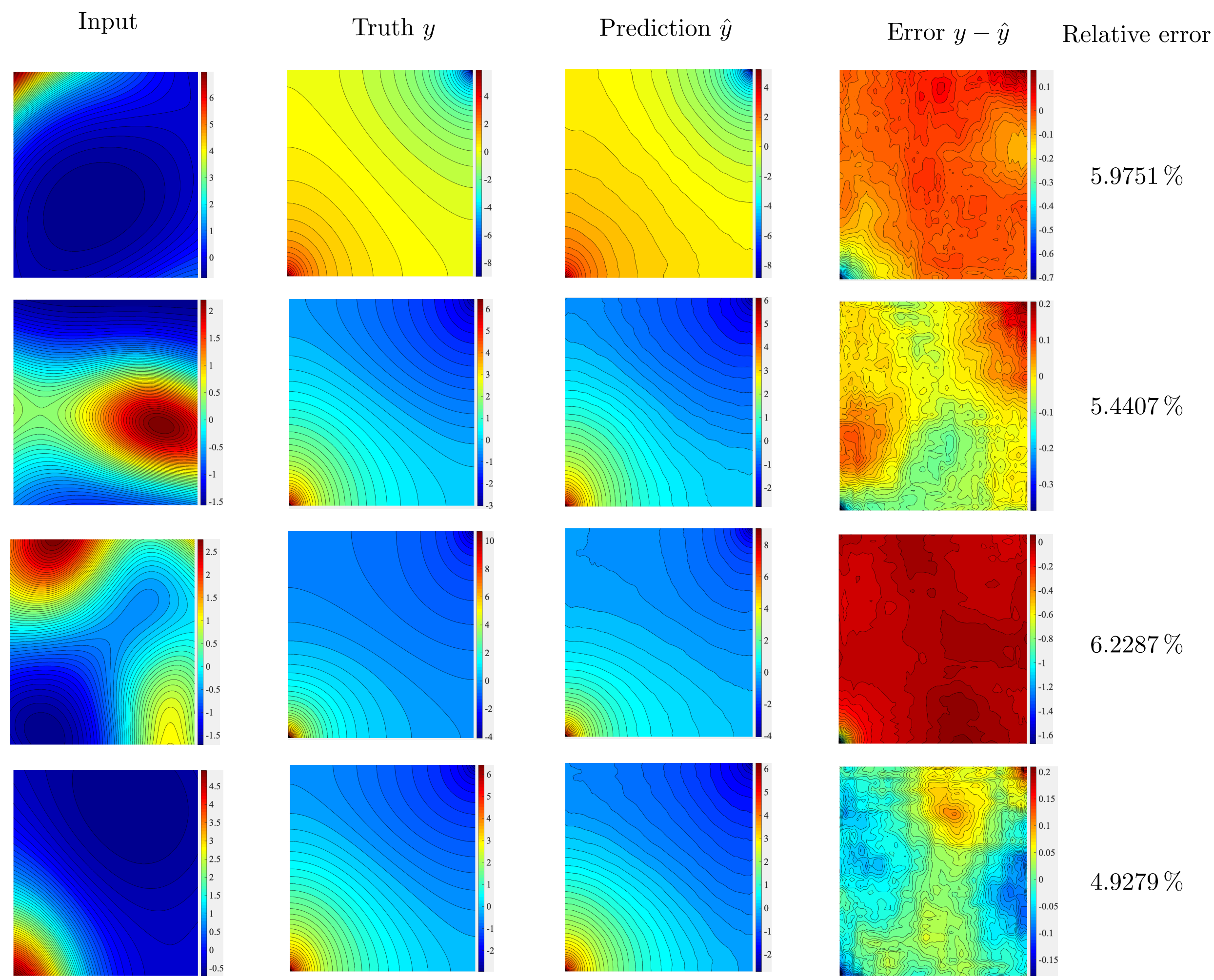

Nonlinear Geometry Analysis

In this example, the complexity of the case study included in the original manuscript is increased. Geometric nonlinearity is considered in the structural analysis and large deformation theory is used. The image-to-image regression approach is used to deal with the prediction of translational displacements from random material properties. For implementation, one only needs to replacement of the training data of FR-21 by nonlinear analysis results and leave everything else unchanged.

Nonlinear FE model. In nonlinear Mindlin plate theory, the inplain strain is partitioned into two parts $\boldsymbol{\epsilon} = \boldsymbol{\epsilon}^l + \boldsymbol{\epsilon}^{non}$, where $\boldsymbol{\epsilon}^l$ describes the linear strain and $\boldsymbol{\epsilon}^{non}$ represents the nonlinear strain term:

$$\boldsymbol{\epsilon}^{non} = \begin{bmatrix} \epsilon_x^{non} \\ \epsilon_y^{non} \\ \gamma_{xy}^{non} \end{bmatrix} = \frac{1}{2} \begin{bmatrix} \left(\frac{\partial u}{\partial x}\right)^2 + \left(\frac{\partial v}{\partial x}\right)^2 + \left(\frac{\partial w}{\partial x}\right)^2 \\ \left(\frac{\partial u}{\partial y}\right)^2 + \left(\frac{\partial v}{\partial y}\right)^2 + \left(\frac{\partial w}{\partial y}\right)^2 \\ 2\left(\frac{\partial u}{\partial x}\frac{\partial u}{\partial y}\right) + 2\left(\frac{\partial v}{\partial x}\frac{\partial v}{\partial y}\right) + 2\left(\frac{\partial w}{\partial x}\frac{\partial w}{\partial y}\right) \end{bmatrix}$$

The solution of these nonlinear equilibrium equations are obtained by the Newton-Raphson (NR) method. The iterative NR process terminates when the unbalanced force residual is smaller than the tolerance $\epsilon = 0.0001$ or the NR algorithm reaches the default maximum iteration $n = 10$. The force and displacement vector is initialized to zero and the increment loads $\Delta_p = p/n$ where $p = 10$ and $n = 10$. Four nodes (Q4) quadrilateral elements are adopted for the finite element analysis.

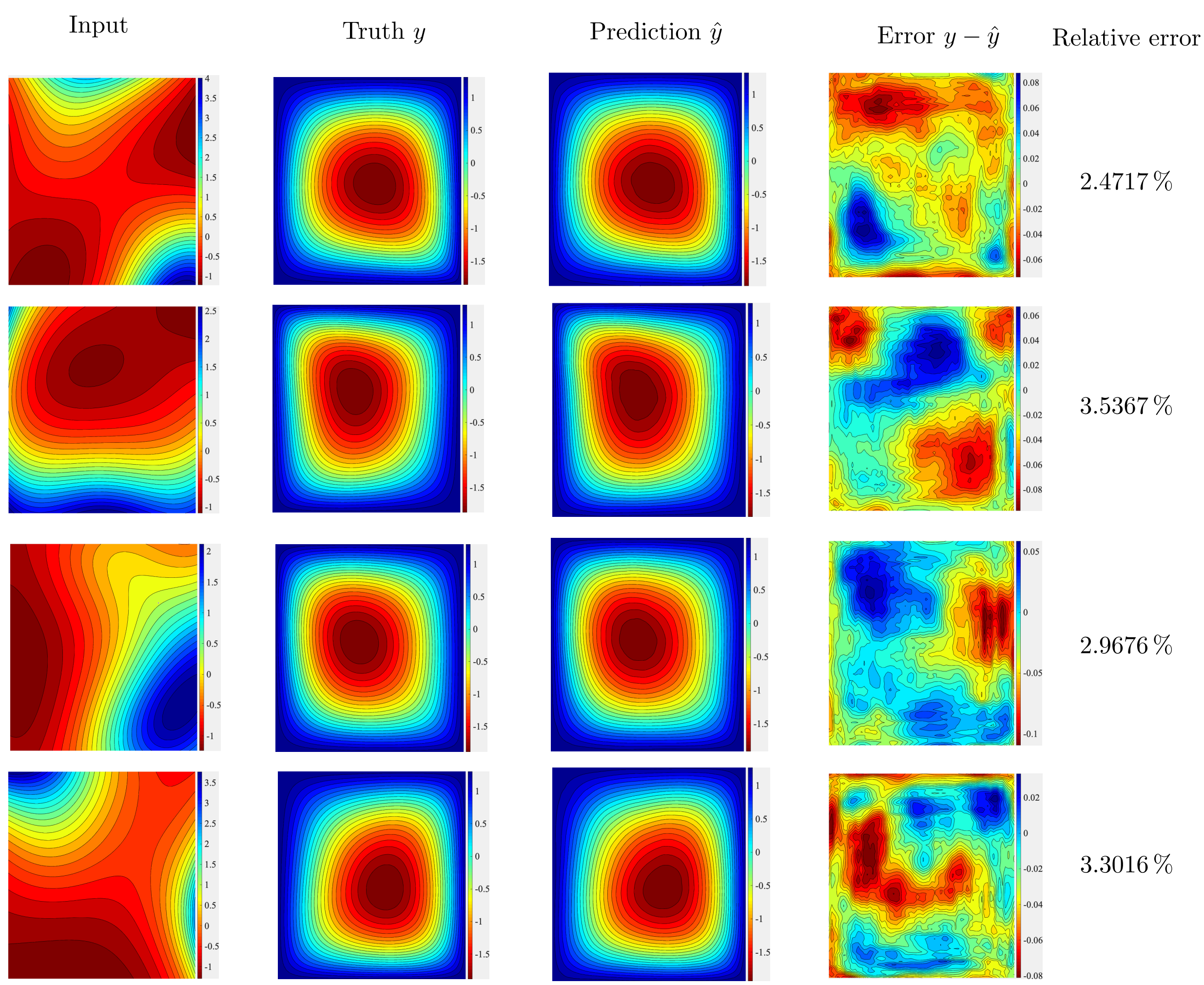

Surrogate model. The field regressor takes the same network architecture introduced in the first case study. The training and test dataset contain 1024 and 200 samples, respectively. To show the prediction performance, 4 test samples are randomly selected and prediction results are summarized in the figure above. The predication results indicate the advanced capability of the proposed deep learning model in terms of dealing with high-dimensional nonlinear systems.

Gaussian & Non-Gaussian Uncertainty Model

In this section, we have tested the proposed surrogate using different uncertainty models. Specifically, we have tested 7 uncertainty models. First, three Gaussian models are considered:

Gaussian Type	$\mathcal{N}(m(x,y), k(x,y))$		
Case 1	$m(x,y) = 5$	$k(x,y) = \exp(-\frac{\|\|x-y\|\|^2}{2\sigma^2})$	Gaussian kernel
Case 2	$m(x,y) = 5$	$k(x,y) = \exp(-\frac{\|\|x-y\|\|}{2\sigma})$	Laplace kernel
Case 3	$m(x,y) = 5$	$k(x,y) = \exp(-\frac{\|\|x-y\|\|^2}{2(\sigma^2 + c_0\|\|x-y\|\|)})$	Hybrid kernel

$$\sigma = \sqrt{1/2} \qquad c_0 = 1$$

The same benchmark FR-21 is used. Part of the prediction results are shown below:

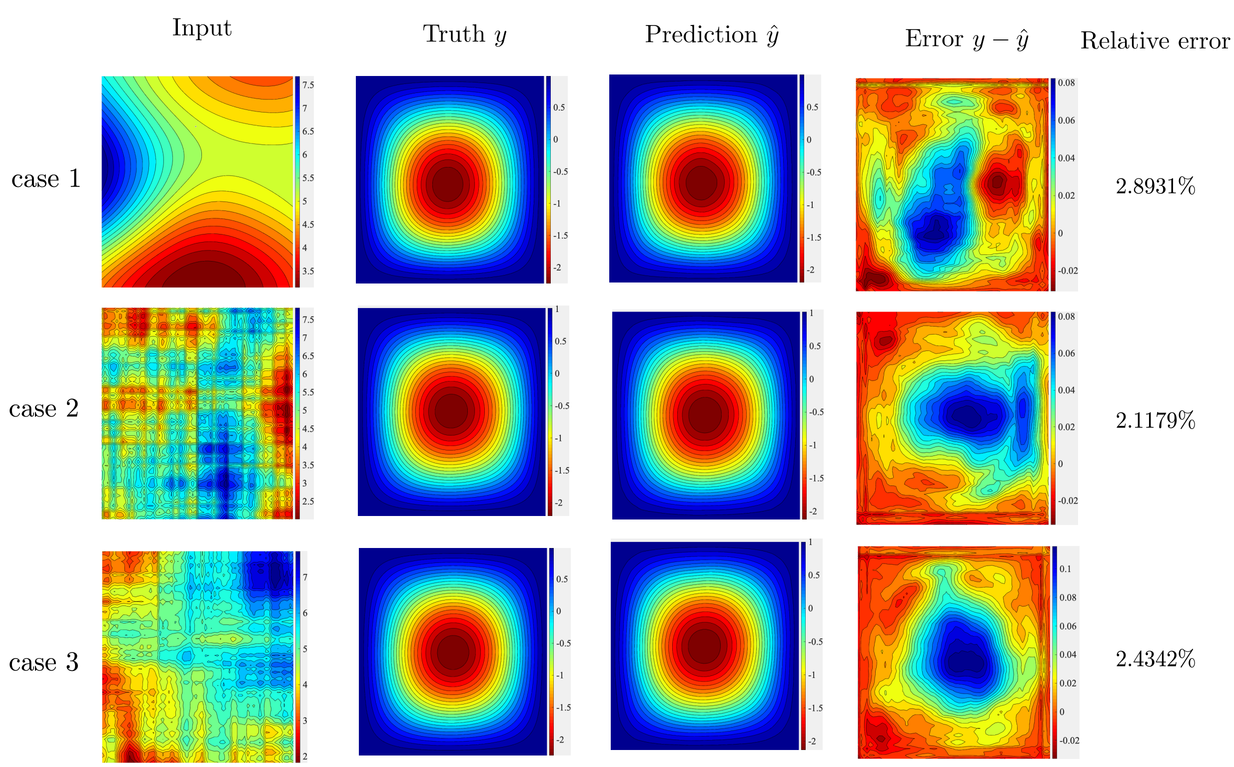

Secondly, four non-Gaussian models have been examined:

Uniform field	$\mathcal{U}[a,b]$		
Case 4	$a=1$	$b=2$	

Lognormal random field		$\exp(\mathcal{N}(m(x,y),k(x,y)))$	
Case 5	$m(x,y)=0$	$k(x,y)=\exp(-\frac{\|\|x-y\|\|^2}{2\sigma^2})$	Gaussian kernel
Case 6	$m(x,y)=0$	$k(x,y)=\exp(-\frac{\|\|x-y\|\|}{2\sigma})$	Laplace kernel
Case 7	$m(x,y)=0$	$k(x,y)=\exp(-\frac{\|\|x-y\|\|^2}{2(\sigma^2+c_0\|\|x-y\|\|)})$	Hybrid kernel
		$\sigma=\sqrt{1/2}$ $\quad c_0=1$	

The prediction results suggest that the model is robust dealing with different types of uncertainties.

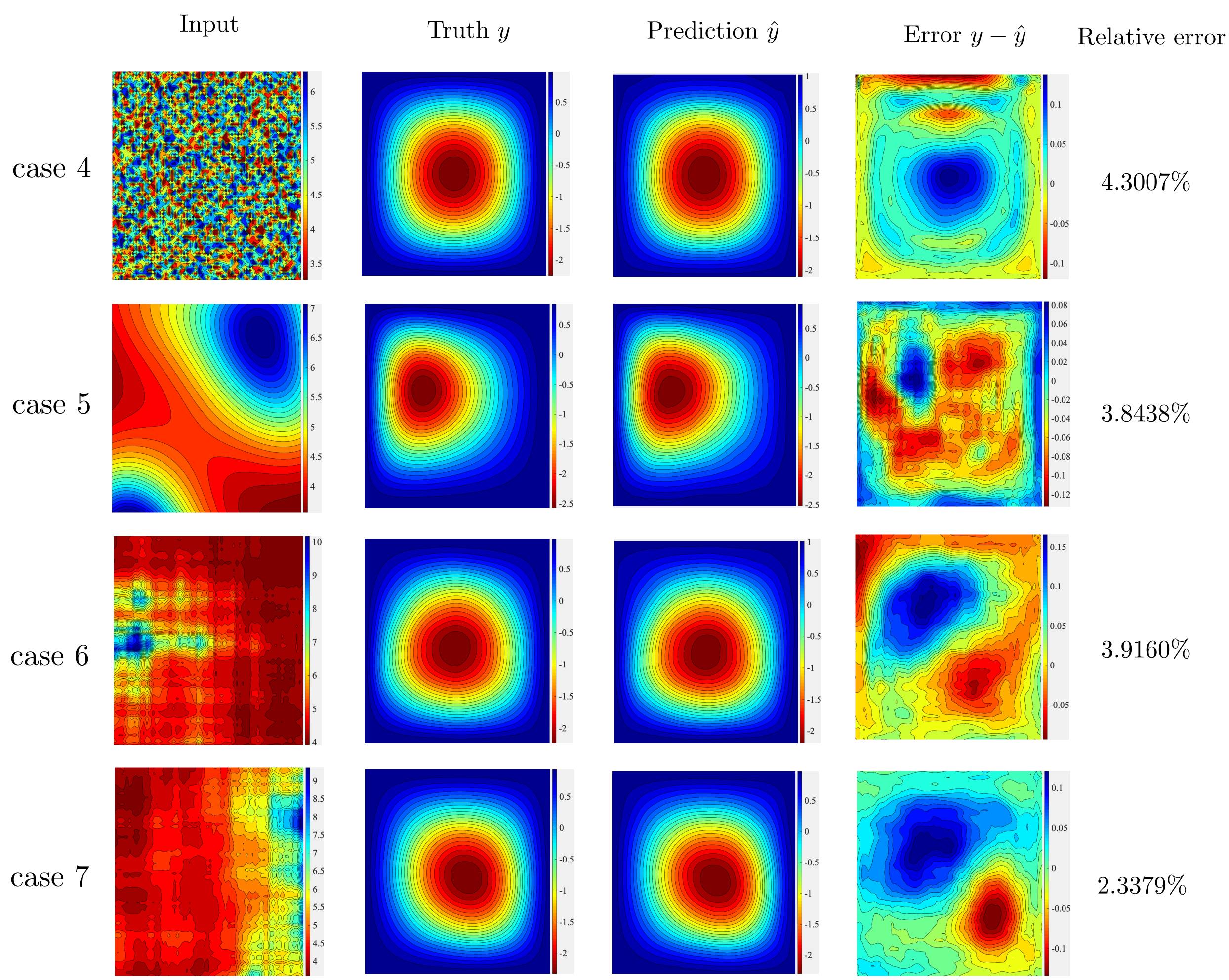

Summary

For the purpose of reproducibility, all the data presented in the manuscript and this supplementary material report will be made available at `https://xihaier.github.io` upon publication of this manuscript.